Journal of Geochemical Exploration 197 (2019) 60–69

Contents lists available at ScienceDirect

Journal of Geochemical Exploration

journal homepage: www.elsevier.com/locate/gexplo

Genesis of Huoqiu banded iron formation (BIF), southeastern North China Craton, constraints from geochemical and Hf-O-S isotopic characteristics

Kejun Hou, Xudong Ma*, Yanhe Li, Feng Liu, Dan Han

MLR Key Laboratory of Metallogeny and Mineral Assessment, Institute of Mineral Resources, Chinese Academy of Geological Sciences, Beijing 100037, China

ARTICLE INFO

Keywords:
Banded iron formation
Geochemistry
In-situ zircon Hf isotopes
Quartz grains O isotopes
Pyrite sulfur isotopes
North China Craton

ABSTRACT

The Huoqiu iron deposit is one of the few Superior-type BIF ore fields in China. To clarify the genesis of Huoqiu BIFs, we give out the geochemical and O-S isotopic data of the BIF samples and zircon Hf isotopic data of the wall-rock. The Huoqiu BIFs show dominant composition of SiO_2 + $Fe_2O_3^T$, and varying contents of Al_2O_3, MgO, CaO, Rb, Sr, Zr and Hf, suggesting their formation mainly through chemical precipitation and incorporation of terrigenous felsic clastics. Shale-normalized rare earth element patterns of the BIF samples show the features characteristic of other Archean and Paleoproterozoic BIFs, with HREE enrichment relative to LREE, positive La and Eu anomalies, and superchondritic Y/Ho ratios comparable to modern seawater. Positive Eu anomalies are attributed to an imprint of high-temperature hydrothermal fluids. None to negative Ce anomaly shown by the BIFs imply the Huoqiu BIFs was precipitated from the mildly oxidized seawater in a nearshore setting. The quartz separated form Huoqiu BIF has $\delta^{18}O_{V\text{-}SMOW}$ values of 11.8‰–14.8‰, within the extent of the siliceous rocks deposited from high-temperature hydrothermal. The $\delta^{34}S$ values of pyrite grains vary from −2.84 to +4.38‰, which is similar as the sulfur derived from mixtures between mantle fluids and sediments; The $\Delta^{33}S$ values varied from −0.08‰ to +1.03‰, imply that the Huoqiu BIFs deposited distally from the volcanic center. The Hf model ages of these detrital zircons from the wall rock give three prominent peak at 3.1–3.0 Ga, 2.9–2.7 Ga and 2.5 Ga, respectively, it suggest that there were three episodes of the crust growth in the Huoqiu area. Integrated these data with the pioneering studies on the Huoqiu BIFs and wall rocks, we confirmed that the Huoqiu BIFs were sourced from the high-temperature hydrothermal related with the volcanics and precipitated from the mildly oxidized seawater in a nearshore setting and distally from the volcanics at 2.5 Ga.

1. Introduction

Banded iron formations (BIFs) are composed of intercalated microcrystalline quartz, iron oxides, and iron-rich silicates within an evaluated total Fe and Si content of 20–40 wt% and 40–60 wt% respectively (e.g. James, 1954; Klein, 2005), and only precipitated in Precambrian era (the age of BIFs ranges from 3.8 Ga to 1.8 Ga, minor reappearing at ca. 0.8–0.6 Ga; Huston and Logan, 2004; Klein, 2005), which are supplied as the principal source of iron for the global steel industry (Bekker et al., 2010). In China, the explored BIFs are mainly distributed in the North China Craton (NCC) (Shen et al., 2005, 2006; Zhai and Santosh, 2011, 2013; Ma et al., 2014).

The Huoqiu iron deposit is one large iron ore field, which is located in the southeastern margin of the NCC, and one of the few Superior-type BIF mines in China (Yang et al., 2014; Liu and Yang, 2015). After decades of efforts in mineral exploration, more than ten large iron deposits have been identified, such as Zhouji, Zhangzhuang, Lilaozhuang, Zhouyoufang, Fanqiao, Wuji and Lilou iron deposits (Fig. 1c, No. 313 Geol. Team, 1991). Although there are several Chinese researcher carrying lots of work on the Huoqiu iron deposit (e.g. Qi, 1987; Liu and Yang, 2015; Yang et al., 2014), compared with other BIF iron deposits in the NCC, several basic questions are being debated on, e.g., the formation age of Huoqiu iron deposit, the tectonic environment of metallogenesis, source of iron (Liu and Yang, 2015).

In this paper, we present geochemical, O-S isotopic characteristics of the Huoqiu BIFs and zircon Hf isotopic data of wall-rocks. These data enable us to constrain the formation and depositional environment of the Huoqiu BIF iron deposit.

2. Geological background

2.1. Regional geology

The NCC is the oldest and largest craton in China, covering an area

* Corresponding author.
E-mail address: maxudong2011@126.com (X. Ma).

https://doi.org/10.1016/j.gexplo.2018.11.005
Received 15 March 2018; Received in revised form 23 October 2018; Accepted 6 November 2018
Available online 16 November 2018
0375-6742/

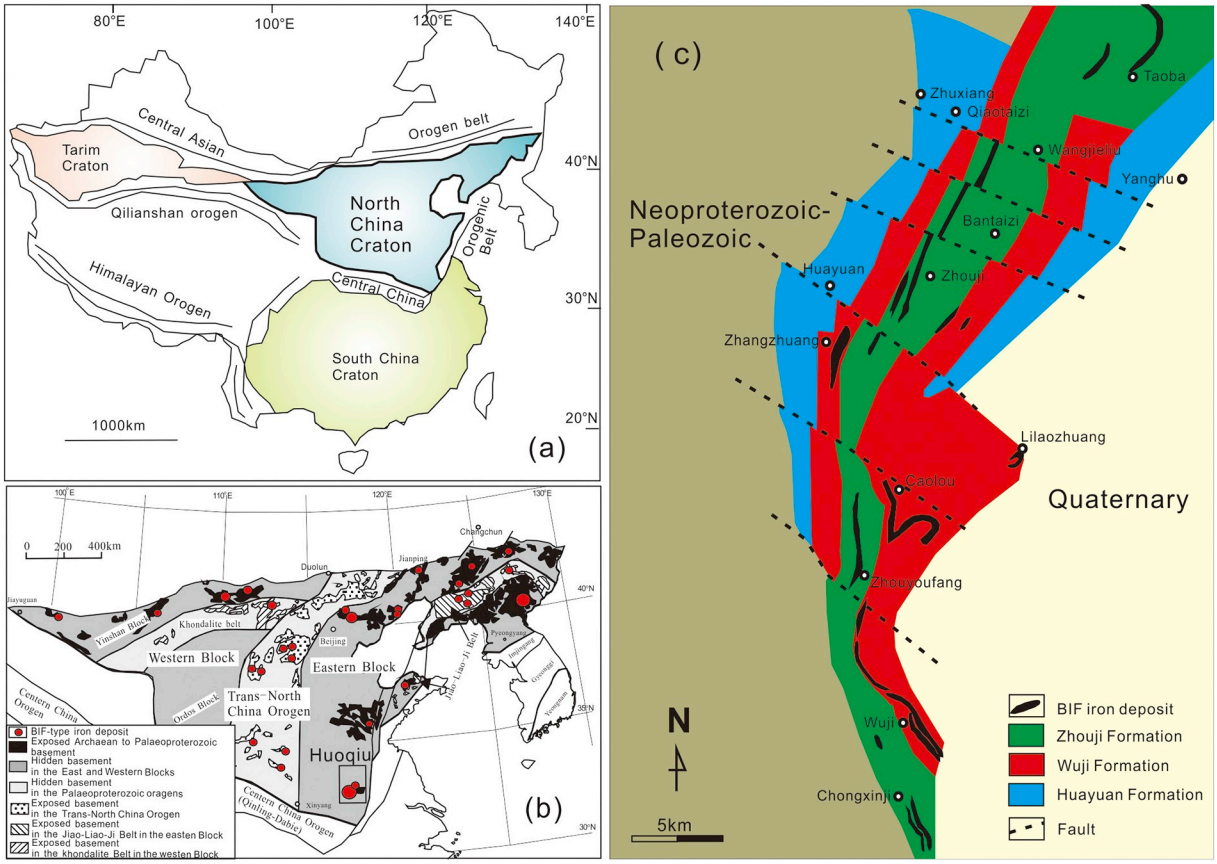

Fig. 1. (a) Tectonic framework of China illustrating the major Precambrian cratons and younger orogens (modified after Zhao et al., 2005); (b) Geological sketch map of the North China Craton showing Precambrian BIF-type iron deposit distribution (modified after Zhao et al., 2005); (c) Geological sketch map of the Huoqiu complex (revised after the No.337 Geol. Team, 1986; No.313 Geol. Team, 1991; Liu and Yang, 2015).

of about 1,500,000 km^2, which was formed by amalgamation of a series of 2.5–3.8 Ga micro-continental blocks (Fig. 1a, b; Zhai and Santosh, 2011; Zhao et al., 2012). However, the number of constituent blocks, when and how they were assembled to form the coherent basement of the NCC remain unresolved, resulting in several models proposed for the tectonic subdivision and amalgamation of the NCC (Zhao et al., 2012, and references therein). One of the models considers that at least seven Archean micro-blocks (named the Jiaoliao, Qianhuai, Ordos, Jining, Xuchang, Xuhuai and Alashan blocks) converged and cratonized into NCC at ca. 2.45 Ga, and subsequently the NCC experienced an orogenic cycle from rifting to subduction-collision along three major Paleoproterozoic orogenic belts (termed the Fengzhen, Liaoji and Jinyu Orogenic belts) during 2350–1970 Ma with following regional high-grade metamorphism at 1950–1820 Ma (Zhai and Santosh, 2011, and references therein). Another highly accepted model is remarkably different, which suggests that four micro-continental blocks (termed the Yinshan, Ordos, Longgang and Nangrim blocks) separated by three Paleoproterozoic tectonic belts (named the Khondalite Belt, Jiao-Liao-Ji Belt and Trans-North China Orogen) constructed the NCC through collision during Paleoproterozoic, among which the Yinshan Block collided with the Ordos Block to form the Western Block along the Khondalite Belt at ca. 1.95 Ga and the Longgang Block collided with the Nangrim Block to form the Eastern Block along the Jiao-Liao-Ji Belt at ca. 1.90 Ga (Fig. 1b; Zhao et al., 2005, 2012). The final cratonization of the NCC was accomplished by the collision between the Eastern and Western blocks along the Trans-North China Orogen at ca. 1.85 Ga (Fig. 1b; Zhao et al., 2005, 2012). Here, we adopted the model proposed by Zhao et al. (2005, 2012), on account of its highly accepted and concision.

The Huoqiu BIF ore field tectonically belongs to the Eastern Block in NCC (Fig. 1b). The Archean basement of the Eastern Block consists of 3.8–2.5 Ga TTG gneisses, ultramafic-mafic igneous rocks and minor supracrustal rocks (Bai and Dai, 1998; Zhao et al., 1998; Nutman et al., 2011; Wan et al., 2012). These rocks became deformed and metamorphosed from greenschist to granulite facies at ~2.5 Ga (Jahn and Zhang, 1984; Bai and Dai, 1998; Kröner et al., 1998; Wang et al., 2012) and have anti-clockwise P-T paths (Zhao et al., 1998, 2012; Zhao and Zhai, 2013; Wu et al., 2012). Numerous U-Pb ages and Hf and Nd isotopic data indicate that the Eastern Block experienced major crustal growth at 2.7–2.8 Ga and remelting at 2.5 Ga (Wu et al., 2005; Jiang et al., 2010; Geng et al., 2012).

The Huoqiu BIF orebodies are mainly hosted in Huoqiu complex, which was named as “Huoqiu group” in the Chinese literature (Figs. 1c and 2, Qi and Yao, 1982; Qi, 1987). The protolith of Huoqiu group is considered to be formed by rhythmic sequences of volcanic-sedimentary cycle and experienced amphibolite facies metamorphism (Ying et al., 1984). According to the rock associations, The Huoqiu group is divided into three formations, namely Huayuan Formation (Fm), the Wuji Formation and Zhouji Formation, and contacted conformably from the bottom up (Fig. 2). The Huayuan Fm is mainly composed of migmatized biotite-hornblende-plagioclase gneiss, plagioclase amphibolite and hornblende-biotite migmatite. The Wuji Fm is divided into two parts, where the lower part is dominated by banded migmatite, migmatized biotite-plagioclase leptynite and hornblende-biotite-plagioclase gneiss, spatially associated with plagioclase amphibolite; the upper part consists of biotite-plagioclase leptynite, schistose garnet-plagioclase-biotite rocks, magnetite quartzite and spatially associated with dolomite marble and plagioclase amphibolite. The Zhouji Fm is

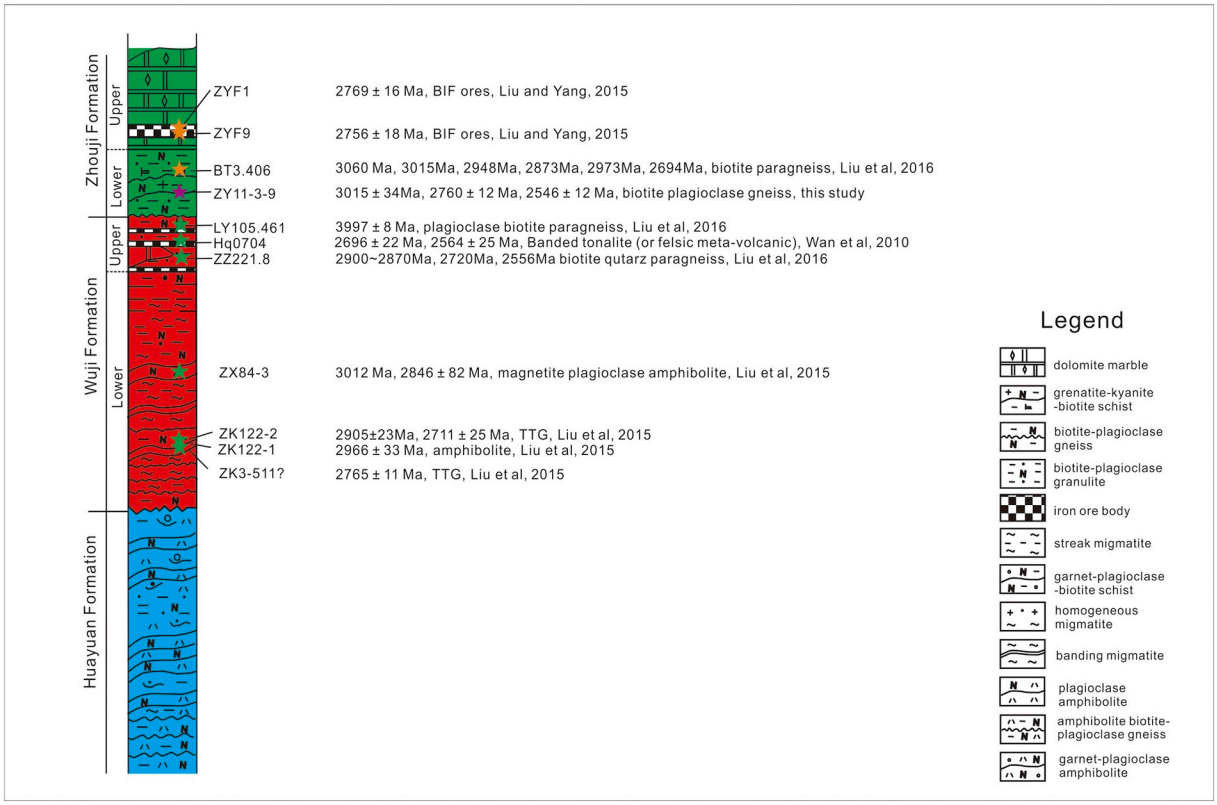

Fig. 2. General stratigraphic column and zircon age of the Huoqiu group (modified from Liu and Yang, 2015).
ZYF1 and ZYF2 are cited from Liu and Yang (2015); BT3.406, LY105.461 and ZZ221.8 are cited from Liu et al. (2016); Hq0704 are cited from Wan et al. (2010); ZX84-3, ZK122-2, ZK122-1 and ZK3-511 are cited from Liu et al. (2015).

divided into two parts, where the lower part is mainly composed of migmatized biotite-plagioclase leptynite, migmatite, biotite-plagioclase gneiss and spatially associated with plagioclase amphibolite and magnetite quartzite; The upper part is represented by dolomite marble, magnetite quartzite and spatially associated with quartz schist.

2.2. Deposit geology

The Huoqiu ore field is composed of > 10 iron deposits with total proven reserves of 2.3 billion tons at 20%–45% Fe (Av. 31% Fe) (No.313 Geol. Team, 1991). The iron ores are subdivided into four types in terms of mineral assemblages: (1) quartz + magnetite; (2) quartz + specularite; (3) magnetite + quartz + silicate (hornblende, iron amphibole–magnesium iron amphibole, actinolite, tremolite, diopside); and (4) quartz + specular hematite iron ore + silicate (hornblende, actinolite, tremolite, diopside).

According to the characteristics of iron oxide, the iron ores were subdivided into hematite (or specularite) and magnetite phase by Yang et al. (2014): (1) Hematite (or specularite) phase. The main ore types include spiegel quartzite, and magnetite-spiegel quartzite. Main mineral often occurs with quartz grains composed of banded iron formation. Specularite occurs mainly in flake-plate and granular states existing in the iron formation; (2) Magnetite phase. The main rock types are composed of quartz, magnetite, and amphibole. Few sulfide minerals were also identified from the BIFs, such as pyrite, pyrrhotite and chalcopyrite (Yang et al., 2014).

3. Sample description and analytical procedures

BIF samples were collected from the Zhouyoufang (ZY) and Caolou (CL) iron deposits (Figs. 1c; 3a, b) and a summary of these samples is given in Tables 3–4. Zircon grains were separated from sample ZY11-3-9 for in-situ Hf isotope and U-Pb age analysis, which is a biotite-plagioclase gneiss interbeded with the iron orebody in ZYF No.3 mine (Fig. 3c, d). Quartz grains separated from nine BIF samples were analyzed for O isotopic compositions, and pyrite grains separated from thirteen BIFs samples were analyzed for S isotopic compositions.

3.1. Geochemical analyses

All geochemical analyses were undertaken at the National Research Center for Geoanalysis, Chinese Academy of Geological Sciences (CAGS), Beijing. The contamination-free samples were pulverized to 200 meshes. Major element oxides were measured by X-ray fluorescence spectrometry (XRF, PW4400). The relative standard derivations of measurements were < 0.5%. Trace elements and REEs were determined using inductively coupled plasma-mass spectrometry (ICP-MS, PE300D). Powered samples were digested in high-pressure Teflon bombs using a mixture of super-pure HF-HNO_3 for 2 days at ~100 °C. The procedure involved evaporation to near dryness, refluxing with super-pure HNO_3, and drying twice, until the powders were completely dissolved. Duplicate analyses of samples and rock standards yielded relative standard derivations of < 5% for most trace elements.

3.2. LA-ICP MS zircon Hf isotopes

Zircon Hf isotope analysis was carried out using a Newwave UP213 laser-ablation microprobe attached to a Neptune multi-collector ICP-MS at the Institute of Mineral Resources, CAGS. Instrumental conditions and data acquisition protocols were described by Hou et al. (2007). A stationary spot used a beam diameter of ~55 μm. As the carrier gas, helium was used to transport the ablated sample mixed with Argon from the laser-ablation cell to the ICP-MS torch by a mixing chamber. $^{176}Lu/^{175}Lu = 0.02658$ and $^{176}Yb/^{173}Yb = 0.796218$ ratios were

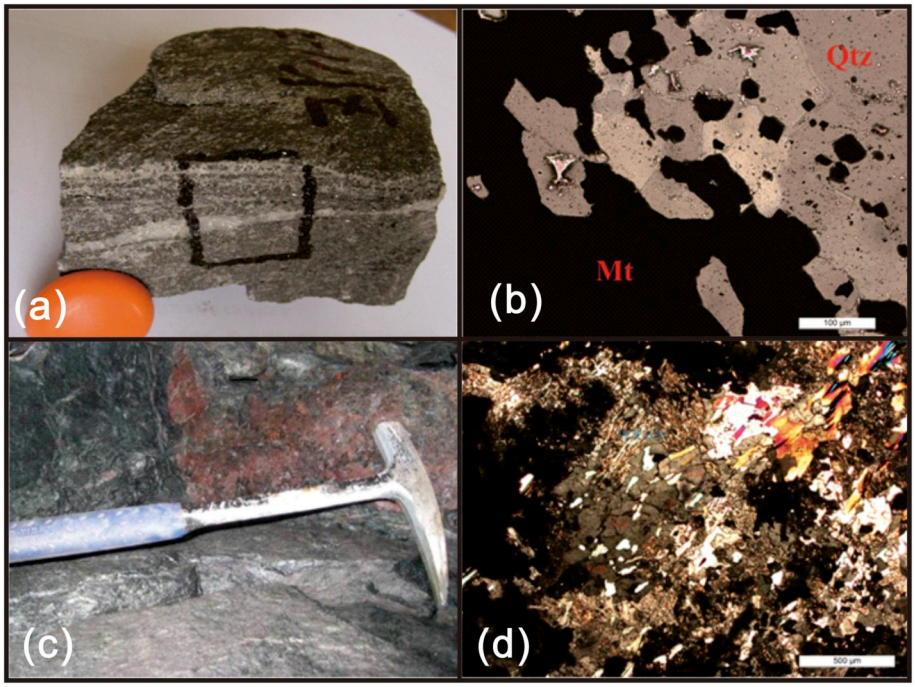

Fig. 3. Photomicrographs of BIF and associated rocks from the Huoqiu iron deposit. (a) Show the BIF ores; (b) show photomicrograph for the BIF ores; (c) The BIF ores and wall rocks of a biotite-plagioclase gneiss; (d) photomicrograph for the wall rocks of a biotite-plagioclase gneiss.

determined to correct for the isobaric interferences of ^{176}Lu and ^{176}Yb on ^{176}Hf. For instrumental mass bias correction Yb isotope ratios were normalized to ^{172}Yb/^{173}Yb = 1.35274 and Hf isotope ratios to ^{179}Hf/^{177}Hf = 0.7325 using an exponential law. The mass bias behavior of Lu was assumed to follow that of Yb, the mass bias correction protocol was described by Hou et al. (2007). Zircon GJ-1 was used as the reference standard, with a weighted mean ^{176}Hf/^{177}Hf ratio of 0.282008 ± 0.000019 (2σ, n = 18). The data were processed using GLITTER and ISOPLOT (Ludwig, 2003) programs.

3.3. Quartz grains O isotopes

Quartz grains were separated prior to O isotope analysis. Oxygen was extracted from the quartz by the conventional BrF_5 method at 500 °C (Clayton and Mayeda, 1963). Oxygen isotope ratios were measured using a Thermo Finnigan MAT 253 mass spectrometer at the Institute of Mineral Resources, CAGS. The results are expressed in δ relative to Vienna Standard Mean Ocean Water (V-SMOW) in per mil 'δ' notations, as follows:

$$\delta^{18}O_{V-SMOW} = [(^{18}O/^{16}O)_{sample}/(^{18}O/^{16}O)_{V-SMOW} - 1] \times 1000$$

The analytical precisions of δ^{18}O measurements were 0.2‰ (1 SD) and 0.1‰ (1 SD), respectively, based on repeated measurements of standard samples.

3.4. Pyrite sulfur isotopes

The sulfur isotope measurements of sulfide were performed on pyrite grains were separated from BIF ores. Sulfide was extracted, and the sulfur isotope composition was determined based on the method of Robinson and Kusakabe (1975). It was then analyzed with a MAT251EM mass spectrometer at the Stable Isotope Laboratory of Institute of Mineral Resources, CAGS. The analytical reproducibility was ± 0.2‰. The sulfur isotope ratios were reported as δ^{34}S and δ^{34} relative to the Caòon Diablo Troilite (CDT), as follows:

$$\delta^{34}S = [(\delta^{34}S/\delta^{32}S)_{sample}/(\delta^{34}S/\delta^{32}S)_{V-CDT} - 1] \times 1000$$

$$\delta^{33}S = [(\delta^{33}S/\delta^{32}S)_{sample}/(\delta^{33}S/\delta^{32}S)_{V-CDT} - 1] \times 1000$$

$$\Delta^{33}S = \delta^{33}S\text{–}1000 \times [(1 + \delta^{34}S/1000)^{0.515} - 1]$$

4. Results

4.1. Major, trace and rare earth elements

Major, trace and rare earth elements are presented in Table s1.

The BIFs from the Huoqiu iron deposit are mainly composed of SiO_2 (26.5–70.0 wt%) and $Fe_2O_3^T$ (11.1–55.4 wt%), with subordinate Al_2O_3 (0.10–4.45 wt%, except for two high values of 12.8 wt% and 13.1 wt%), MgO (0.04–5.59 wt%, except for two calcite-bearing samples of 8.45 wt % and 13.5 wt%) and CaO (0.10–3.99 wt%, except for two calcite-bearing samples 22.2 wt% and 7.58 wt%). Other elements such as K_2O (0.00–2.35 wt%), Na_2O (0.01–1.88 wt%, except for an amphibole-bearing sample of 4.98 wt%), TiO_2 (0.01–0.29 wt%), MnO (0.01–0.43 wt%) and P_2O_5 (0.00–0.15 wt%) are minor.

The total REEs concentration (ΣREE) of each sample widely varies between 3.07 ppm and 199 ppm. Except for two Fe-poor samples, the others are characterized by depletion of light REE relative to heavy REE (La/Yb_{PAAS} = 0.08–0.83, averaging at 0.53). The BIFs also are characterized by strong positive Eu_{PAAS} anomalies (up to 12.7) and weak negative or no Ce_{PAAS} anomalies (Ce/Ce^*_{PAAS} = 0.79–1.04). The Y/Ho ratios are high (27.3–53.0, average of 38).

4.2. Zircon Lu-Hf isotopes

The Hf isotope results are listed in Table s2 and shown in Fig. 4, initial ^{176}Hf/^{177}Hf ratios, εHf(t) values and depleted mantle model ages (T_{DM}) were calculated based on the ^{207}Pb/^{206}Pb age of individual detrital zircons.

The εHf(t) values show a large variation from −20.56 to +7.05. In particular, most $\varepsilon Hf_{(t)}$ values are positive, indicating that their source rocks are derived from juvenile crust and/or depleted mantle. The single stage Hf model ages (T_{DM1}) of these detrital give three prominent peak at 3.1–3.0 Ga, 2.9–2.7 Ga and 2.5 Ga, suggesting multistage crustal growth in the Huoqiu area.

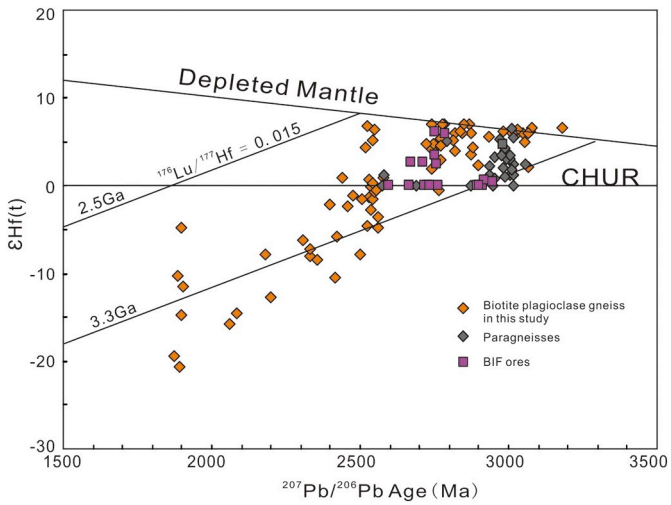

Fig. 4. εHf(t) vs. age diagram for zircon samples from the sample ZY11-3-9 and the BIF ores and wall rocks. The data for the BIF ores and paragneiss are from Liu and Yang (2015).

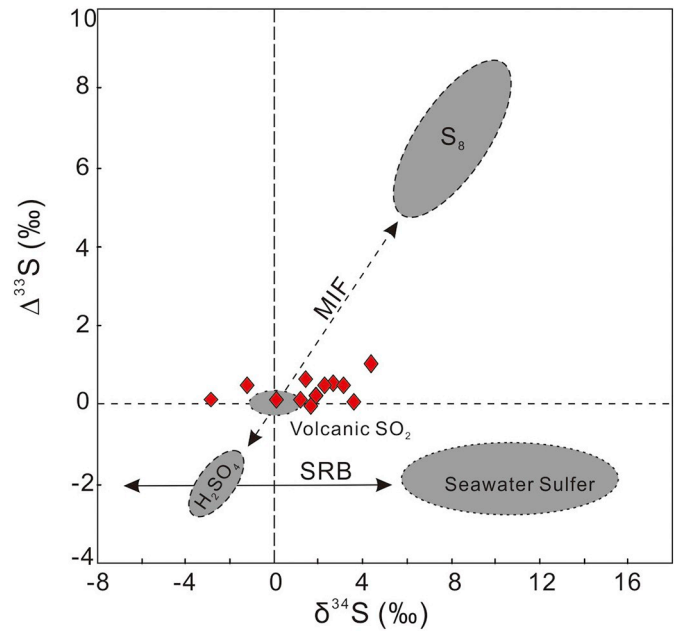

Fig. 5. Multiple sulfur isotope systematics for the pyrite in the Huoqiu BIFs. Atmospheric MIF and mass-dependent fractionation by sulfate reducing bacteria (SRB) is shown in dashed and solid arrows, respectively. Gray fields represent isotopic composition of volcanic SO_2, S_8 and H_2SO_4 aerosols, and seawater sulfate (SS).

4.3. Quartz O isotope compositions

The O isotope compositions of quartz from ten BIF samples analyzed during this study are given in Table s3. The quartz separates also have $\delta^{18}O_{V\text{-}SMOW}$ values of 11.8‰ to 14.8‰, with an average of 12.9‰, falling between values for quartz within igneous rocks and values for marine siliceous rocks, similar to siliceous rocks that formed during hydrothermal activity (Li and Jiang, 1995; Li et al., 2014).

4.4. Sulfur isotope compositions

The measured sulfur isotopic values for twelve pyrites in BIFs are listed in Table s4. The $\delta^{33}S$ varied from −1.39 to +3.28, $\delta^{34}S$ varied from −2.84 to +4.38‰ and the $\Delta^{33}S$ varied from −0.08 to +1.03. In the Fig. 5, the samples all plot around the volcanic sulfur area and follow the bacterial reduction of seawater (SRB) trend.

5. Discussion

5.1. Material source of the Huoqiu BIF

According to the major compositions of iron oxides and silica coupled with quite minor other oxides (e.g., Al_2O_3, MgO and alkalis) in most BIFs, it is consensus that the BIF are formed by chemical precipitation (James, 1954; Trendall, 2002). However, not all BIFs represent entirely pure chemical sediments, many BIFs are commonly contaminated by clastic components (Lan et al., 2014 and references therein). The Huoqiu BIFs are of high contents of $SiO_2 + Fe_2O_3^T$ (74.2–100 wt%, average at 91.3 wt%), implying they were mainly originated from chemical precipitation like other BIFs. Since both Al_2O_3 and TiO_2 cannot be introduced in solution, the contents of Al_2O_3, TiO_2 are usually chosen as indicators for evaluating the addition of clastic components (e.g. Basta et al., 2011; Ewers and Morris, 1981; Pecoits et al., 2009), which would enhance the $Al_2O_3 + TiO_2$ values up to > 2% (Kato et al., 1996). The high Al_2O_3, TiO_2 contents in the Huoqiu BIF ($Al_2O_3 + TiO_2$ up to 13.39%), suggest there were conspicuous clastic components added into the Huoqiu BIF. Compared with the typical Y/Ho ratios of seawater (43–80, Nozaki et al., 1997), their relatively lower and widely varying Y/Ho ratios (27.3–53.0, average of 38) also indicate that the Huoqiu BIF have been subjected to detritus contamination, because minor admixtures of contaminants in chemical sediments precipitating from seawater would depress seawater-like super-chondritic Y/Ho ratios (Bolhar et al., 2004). This inference is confirmed by the negative correlation between Y/Ho ratio and Al_2O_3 content (Fig. 6a). The strongly positive correlation between Al_2O_3, TiO_2 and ΣREE (Fig. 6b, c, d) is the third evidence for the incorporation of detrital components contributing to the chemical precipitate (Basta et al., 2011 and references therein). Moreover, Zr, Hf, Rb, Y, and Sr are commonly derived from the weathering of crustal felsic rocks, whereas Cr and Ni call for a mafic source (Gnaneshwar Rao and Naqvi, 1995; Sunder Raju, 2009). The evidently positive correlation between TiO_2 and Zr, Al_2O_3 and Zr, Y and Zr, as well as Hf and Zr (Fig. 6e, f, g, and h) suggest that these materials were derived from felsic crustal sources. On the contrary, the lack of clear correlation between MgO and Cr as well as MgO and Ni suggests that mafic source detritus was minor (Fig. 7a, b).

Intense positive Eu anomalies (Fig. 8) are also shown by the Huoqiu BIF, which could not be inherited from seawater (Alibo and Nozaki, 1999; Freslon et al., 2011; Zhang and Nozaki, 1996). Since neither diagenetic nor metamorphic conditions are instrumental in decoupling of Eu from the other REY (Bau and Dulski, 1996; Lan et al., 2014), other sources characterized by remarkably positive Eu anomalies should be involved during the deposition of the Huoqiu BIFs. Hydrothermal fluids have been widely considered as the sources responsible for positive Eu anomalies in BIFs (e.g., Danielson et al., 1992; Douville et al., 1999; Klinkhammer et al., 1994; Lan et al., 2014; Wang et al., 2014). The strongest positive Eu anomaly in the Huoqiu BIF is up to 12.7, which suggest that high-temperature hydrothermal fluids should play an important role in the deposition of the Huoqiu BIF. In Al_2O_3-SiO_2 discrimination diagram (González et al., 2009; Wonder et al., 1988), most of the samples from the Huoqiu BIF plot in the hydrothermal field (Fig. 9a). Sm/Yb ratios combining with Y/Ho ratios are used to define the range of hydrothermal fluids and seawater. In Sm/Yb ratios vs. Y/Ho ratios plotting, the samples plot along and under the line of the high-temperature hydrothermal fluids and seawater mixing (Fig. 9b). Part of samples plot under the mixing line due to terrigenous input as an additional REY source, which would have resulted in a decrease of Y/Ho ratios and an increase of Sm/Yb ratios (Wang et al., 2014).

In addition, the quartz in Huoqiu BIF has $\delta^{18}O_{V\text{-}SMOW}$ values of

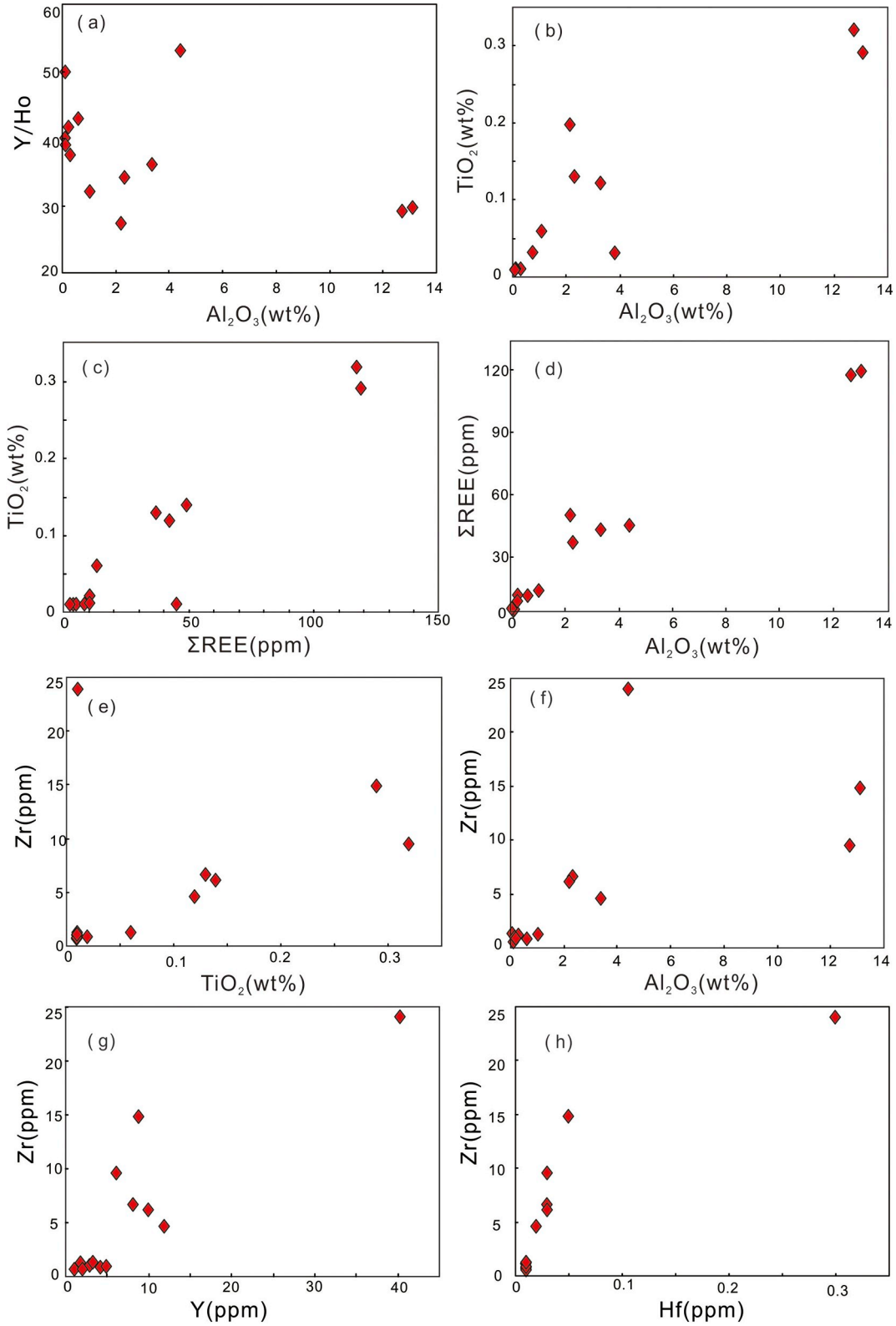

Fig. 6. Covariant relationship between(a) Al_2O_3 and Y/Ho; (b) TiO_2 and $Al2O_3$; (c) TiO_2 and ΣREE (d) Al_2O_3 and ΣREE; (e) TiO_2 and Zr; (f) Al_2O_3 and Zr; and (g) Y and Zr, (h) Hf and Zr showing felsic detrital input.

11.8‰ - 14.8‰, with an average of 12.9‰. Although the Huoqiu BIF has undergone amphibolite facies metamorphism, this metamorphism and hydrothermal fluid exchange are likely to have decreased rather than increased quartz $\delta^{18}O_{V\text{-}SMOW}$ values (Knauth, 2005; Knauth and Lowe, 2003; Robert and Chaussidon, 2006), which indicates that the original $\delta^{18}O_{V\text{-}SMOW}$ value of quartz within the Huoqiu BIF is likely to have been higher than the values determined during this study. These values are similar to siliceous rocks formed by high-temperature hydrothermal sedimentation (Li and Jiang, 1995; Hou et al., 2014). The $\delta^{34}S$ values of pyrite grains vary from −2.84 to +4.38‰, which is

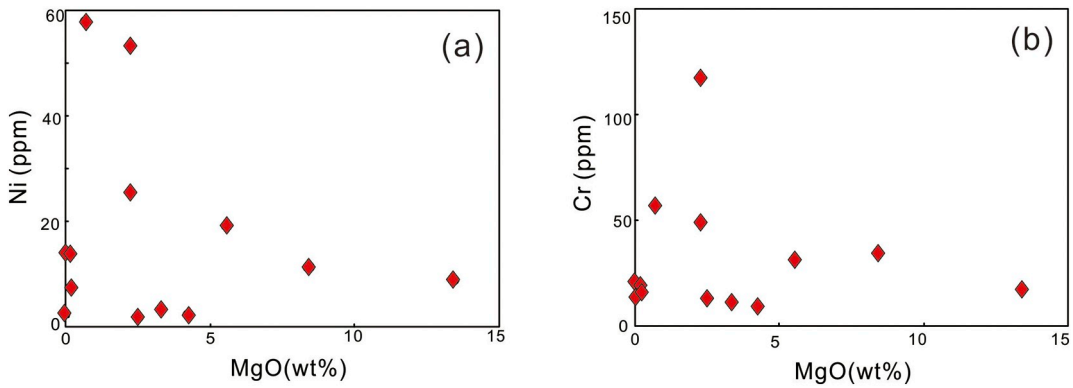

Fig. 7. Binary diagrams of (a) MgO vs. Cr and (b) MgO vs. Ni.

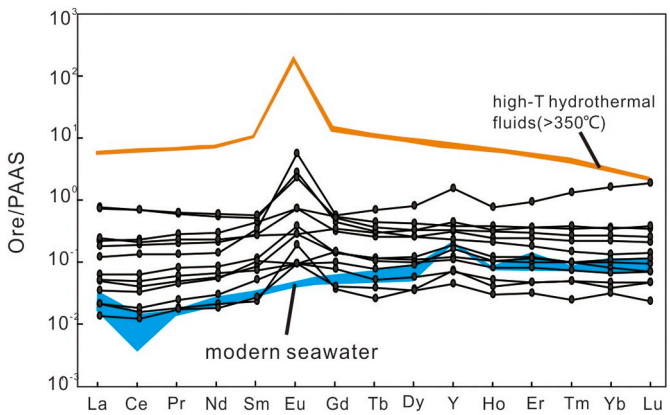

Fig. 8. (a) PAAS-normalized REY pattern. The average compositions of average high-T (> 350 °C) hydrothermal fluids from Bau and Dulski (1999). The range of modern seawater composition is from Bolhar et al. (2004).

similar as the sulfur derived from mixtures between mantle fluids and sediments (Hoefs, 2009).

5.2. Depositional environment

REEs are also used to trace the depositional environment of the BIFs. The REEs distribution patterns of the Huoqiu BIF show LREEs depletion, positive La and Y anomalies, which are the features of seawater, suggesting that the Huoqiu BIF was direct precipitated from seawater (e.g., Alibo and Nozaki, 1999; Bolhar et al., 2004; Freslon et al., 2011; Nozaki et al., 1997; Sholkovitz et al., 1994; Zhang and Nozaki, 1996).

Ce anomaly is usually used to estimate the redox state of the seawater, since Ce^{3+} will be oxidized to Ce^{4+} in an oxidation environment, which has a lower solubility and is tend to be absorbed by suspended particles in seawater, thus leading to a negative Ce anomaly in oxygenated seawater (German et al., 1990; Sholkovitz et al., 1994; Byrne and Sholkovitz, 1996; Bekker et al., 2010). In modern environments, negative Ce anomalies are dominantly produced by Ce scavenging onto Fe-Mn nodules and crusts in deep, oxygenated ocean waters (Bau and Dulski, 1996; Bau, 1999; Slack et al., 2007), however, the similar mechanism couldn't operate during Archean, because the atmosphere and ocean contained little or no oxygen (e.g. Farquhar et al., 2001). After multiple studies using trace element and stable isotope data, it is accepted that the low oxygen levels have locally or episodically arisen in nearshore settings during the Archean (e.g., Anbar et al., 2007; Kaufman et al., 2007; Reinhard et al., 2017; Olson et al., 2013; Planavsky et al., 2014; Riding et al., 2014; Fralick and Riding, 2015; Lalonde and Konhauser, 2015), Thus, German et al. (1991) and Slack et al. (2007) proposed a model for Archean negative Ce anomalies: Fe-Mn-rich particles generated in local, shallow oxidized environments (and producing negative Ce anomalies in the upper part of the water column) would have been dissolved below the redoxcline in deeper waters, returning the Ce back to the seawater and erasing any negative Ce anomaly. Bau and Dulski (1996) suggest that Ce negative anomalies could also be related to a La abnormality, thus they introduced Ce/Ce* versus Pr/Pr* relationships to judge whether there is a Ce negative anomaly. As shown in Fig. 10, part of Huoqiu BIFs show negative Ce anomaly, with the addition of the relatively high MnO content, it suggest that the Huoqiu BIF was precipitated from the mildly oxidized seawater in a nearshore settings.

Sulfur isotope ratios of Archean sulfide and sulfate minerals exhibit signatures of mass-independent fractionation (S-MIF) that are measured

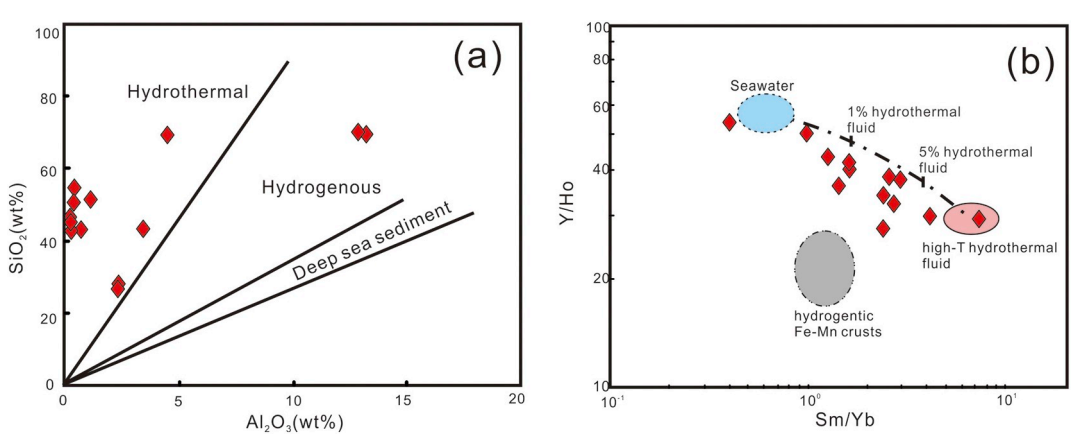

Fig. 9. (a) Al_2O_3 vs. SiO_2 for the BIF ores (modified from Wonder et al., 1988), (b) Two-component conservative mixing lines of Sm/Yb vs. Y/Ho ratios (modified from Alexander et al., 2008).

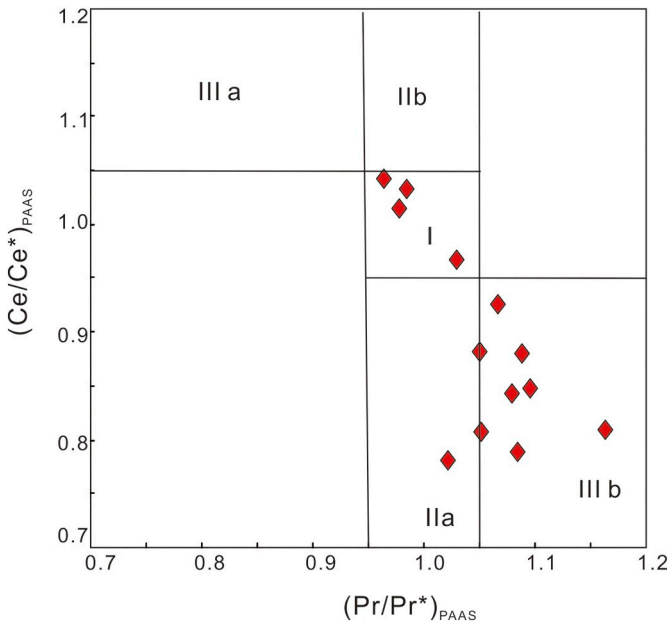

Fig. 10. Plot of $(Ce/Ce^*)_{PAAS}$ vs. $(Pr/Pr^*)_{PAAS}$ (after Bau and Dulski, 1996) for the Huoqiu BIF. Field I: neither Ce_{PAAS} nor La_{PAAS} anomaly; Field IIa: positive La_{PAAS} anomaly, no Ce_{PAAS} anomaly; Field IIb: negative La_{PAAS} anomaly, no Ce_{PAAS} anomaly; Field IIIa: positive Ce_{PAAS} anomaly; Field IIIb: negative Ce_{PAAS} anomaly. The values of the Archean and early Paleoproterozoic BIFs (after Planavsky et al., 2014) and the Neoproterozoic BIFs (after Basta et al., 2011) are shown for comparison.

as deviations from mass-dependent relationships among three isotope ratios of sulfur, which result in non-zero $\Delta^{33}S$ (Ono et al., 2003, 2009 and references therein). The S-MIF signatures are thought to have originated from sulfur photochemical reactions in an anoxic atmosphere (Thiemens, 1999; Farquhar et al., 2000, 2013; Pavlov and Kasting, 2002; Bekker et al., 2004). In an anoxic Archean atmosphere, The volcanic sulfur species were transferred into aerosols of both S_8 and H_2SO_4 by photochemical reactions, the S_8 carried positive $\Delta^{33}S$ and lower $\delta^{34}S$ values, whereas H_2SO_4 carried negative $\Delta^{33}S$ and high $\delta^{34}S$ values into the oceanic sulfur reservoirs (Farquhar et al., 2000, 2013; Ono et al., 2003). The sulfate (H_2SO_4) is easier to soluble into water, thus the sulfate (H_2SO_4) aerosols is quickly removed from the atmosphere by rainout and wet deposition, and deposited around the volcanic center, by contrast, the S_8 is not easy soluble into water, which made the S_8 can be carried a long distance by the atmosphere, and deposited far from the volcanic center (Thiemens, 1999; Farquhar et al., 2000, 2013; Pavlov and Kasting, 2002; Bekker et al., 2004). This conclusion is well confirmed by the sulfur isotope results of the BIFs, The BIFs of Algoma type, which are associated with volcanic or volcaniclastic rocks and near volcanic center, have negative $\Delta^{33}S$ value (−1.55‰ ~ +0.54‰), while those of Superior type, which are associated with clastic-carbonate rocks and distally from the volcanic center, have positive $\Delta^{33}S$ value (−0.13‰ ~ +1.21‰) (Li et al., 2010). The $\Delta^{33}S$ values varied from −0.08‰ to +1.03‰ for the pyrite in Huoqiu BIFs (Fig. 5), which is according with the Superior type, imply that the Huoqiu BIF deposited distally from the volcanic center and these sulfur sources of the BIFs formed in an oxygen-deficient atmosphere.

5.3. Tectonic setting and depositional process for Huoqiu BIF

The Huoqiu BIFs are mainly hosted in the Zhouji and upper Wuji Formation (Fig. 2b), which is composed of metamorphic volcanic-sedimentary cycle (Chen et al., 1988). The meta-sedimental rocks were reconstructed into argillaceous rocks, argillaceous sandstone, graywacke and magnesium carbonate sandwiched between ferrosilicon sedimentary formations (Fig. 2b, Qiu and Yang, 1982; Yang et al., 2014). Liu and Yang (2015) reported the amphibolites interlayered with Huoqiu BIF bands, whose protolith are restored into basaltic volcanics. These basaltic interlayers are subalkaline tholeiites, enriched in LREE and Pb, and depleted in HFSEs, these geochemical features are similar to those of island arc basalt or continental basalt (Yang et al., 2014; Liu and Yang, 2015).

The detrital zircon from the Zhouji and upper Wuji Formation show a complicated U-Pb age distribution, five groups as 4.0 Ga,3.06–3.01 Ga, 2.96–2.90 Ga,2.87–2.72 Ga and 2.56–2.54 Ga (Fig. 2) and document a ~1.8 Ga middle grade regional metamorphism. In this study, the Hf model ages of these detrital zircons give three prominent peak at 3.1–3.0 Ga, 2.9–2.7 Ga and 2.5 Ga (Fig. 3), this result are according with the four younger group of the detrital zircons' ages, suggesting these sediments should be both sourced from vast exposed cratonic basements (Wan et al., 2010; Yang et al., 2012; Liu and Yang, 2015; Liu et al., 2015, 2016) and juvenile magmatic rocks (~2.5 Ga, Wan et al., 2010; Liu and Yang, 2015) like deposited in a back-arc basin or an intra-continental rift. The top of Huoqiu group developed around 500 m thickness of magnesium enriched carbonate rocks, which are general deposited in lagoon or semi-enclosed basin within intra-continent (Fig. 2b, Qiu and Yang, 1982; Yang et al., 2014). As discussed in Sections 5.1 and 5.2, only a certain amounts of felsic terrestrial but no mafic clastic adding and mildly oxidized surface seawater during the BIF formation both call for a nearshore settings.

Continuous high-temperature hydrothermal fluids with the volcanics, the $\delta^{34}S$ and $\Delta^{33}S$ values of Huoqiu BIF and basaltic interlayers within the Huoqiu BIF imply that there was continuous mantle-derived magma during the BIF formation. The youngest age of the detrital zircons is 2.56–2.54 Ga, thus the Huoqiu BIF should be deposited ≤2.54 Ga, however, there is no continuous mantle-derived magma documented during 2.54 Ga ~ 1.8 Ga. Coincidently, there were intense crustal growth and magmatism during ~2.5 Ga (this study and Wan et al., 2010; Liu and Yang, 2015), thus this period is the most possible form Huoqiu BIF formation.

Put all the elements together, we suggest that the Huoqiu BIF was

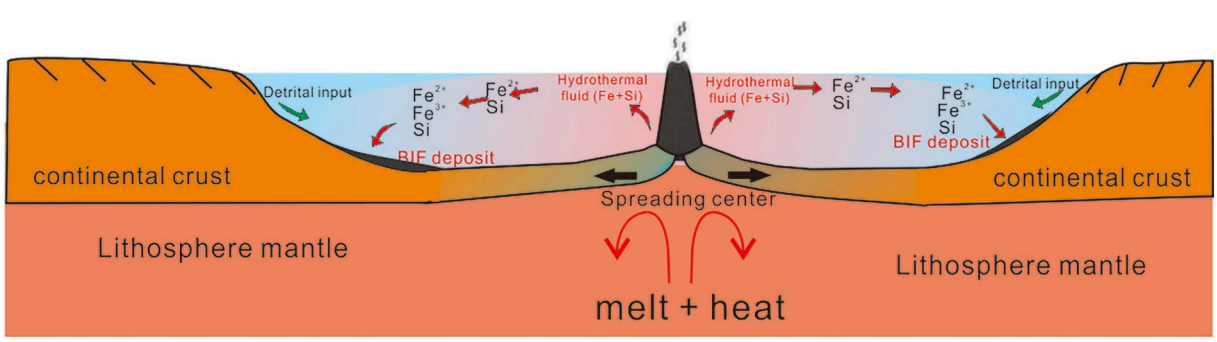

Fig. 11. Schematic diagram showing tectonic evolution of Huoqiu complex and depositional model for the Huoqiu BIF.

deposited in intra-continental rift at ~2.5 Ga. A complete process can be proposed for the Huoqiu BIFs as Fig. 11. A crust spreading happened in intra-continental rift. Along the spreading center, abundant hydrothermal fluid dissolving Fe^{2+} and Si flowed in Archean anoxic seawater, and then the Fe^{2+} and Si would be transported to the shallow-water environment following the cold and heat water convection. In the shallow-water environment, the surface seawater is mildly oxidized, the dissolving Fe^{2+} and Si would deposit into BIF, due to oxygenation of Fe^{2+} to Fe^{3+}.

6. Concluding remarks

The Huoqiu iron deposit is one of large BIF-type ore fields in China, and hosted in the middle-grade metamorphic Huoqiu group. The ores of Huoqiu BIFs show dominant composition of $SiO_2 + Fe_2O_3^T$, and varying contents of major elements and trace elements suggest their formation mainly through chemical precipitation and incorporation of felsic clastics. The REEs show LREE depletion, positive La and Y anomalies as the seawater-like signatures. Intense positive Eu anomalies reflect the participation of hydrothermal fluids. The $\delta^{18}O_{V\text{-}SMOW}$ values of the quartz in ores are according with the siliceous rocks deposited from high-temperature hydrothermal. The $\Delta^{33}S$ values and no Ce anomaly to negative Ce anomaly, imply that the BIFs deposited distally from the volcanic center and precipitated from the mildly oxidized seawater in a nearshore setting. Combined the Hf model age and U-Pb age of detrital zircon from wall rock with the deposited process and environment, we presumed the Huoqiu BIF formed at ~2.5 Ga.

Acknowledgements

This work was financed by the National Natural Science Foundation of China (41373013, 41473014, 40803001, 40273008, 41572174), the National Basic Research Program of China (2012CB416801, 2012CB4146801), and Fundamental Research Funds for Central Scientific Research Institutes (K1404).

Appendix A. Supplementary data

Supplementary data to this article can be found online at https://doi.org/10.1016/j.gexplo.2018.11.005.

References

Alexander, B.W., Bau, M., Andersson, P., Dulski, P., 2008. Continentally-derived solutes in shallow Archean seawater: rare earth element and Nd isotope evidence in iron formation from the 2.9 Ga Pongola Supergroup, South Africa. Geochim. Cosmochim. Acta 72, 378–394.
Alibo, D.S., Nozaki, Y., 1999. Rare earth elements in seawater: particle association, shale normalization, and Ce oxidation. Geochim. Cosmochim. Acta 63, 363–372.
Anbar, A.D., Duan, Y., Lyons, T.W., Arnold, G.L., Kendall, B., Creaser, R.A., Kaufman, A.J., Gordon, G.W., Scott, C., Garvin, J., Buick, R., 2007. A whiff of oxygen before the great oxidation event? Science 317, 1903–1906.
Bai, J., Dai, F.Y., 1998. Archaean crust of China. In: Precambrian Crustal Evolution of China. Springer Geological Publishing House, Beijing, pp. 15–86.
Basta, F.F., Maurice, A.E., Fontbotéc, L., Favargerd, P.Y., 2011. Petrology and geochemistry of the banded iron formation (BIF) of Wadi Karim and Um Anab, Eastern Desert, Egypt: implications for the origin of Neoproterozoic BIF. Precambrian Res. 187, 277–292.
Bau, M., 1999. Scavenging of dissolved yttrium and rare earths by precipitation iron oxyhydroxide: experimental evidence for Ce oxidation, Y-Ho fractionation, and lanthanide tetrad effect. Geochim. Cosmochim. Acta 63, 67–77.
Bau, M., Dulski, P., 1996. Distribution of yttrium and rare-earth elements in the Penge and Kuruman iron-formations, Transvaal Supergroup, South Africa. Precambrian Res. 79, 37–55.
Bau, M., Dulski, P., 1999. Comparing yttrium and rare earths in hydrothermal fluids from the Mid-Atlantic Ridge: implications for Y and REE behaviour during near-vent mixing and for the Y/Ho ratio of Proterozoic seawater. Chem. Geol. 155, 77–90.
Bekker, A., Holland, H.D., Wang, P.L., Rumble Iii, D., Stein, H.J., Hannah, J.L., Coetzee, L.L., Beukes, N.J., 2004. Dating the rise of atmospheric oxygen. 427 (6970), 117.
Bekker, A., Slack, J.F., Planavsky, N., Krapež, B., Hofmann, A., Konhauser, K.O., Rouxel, O.J., 2010. Iron formation: the sedimentary product of a complex interplay among mantle, tectonic, oceanic, and biospheric processes. Econ. Geol. 105, 467–508.
Bolhar, R., Kamber, B.S., Moorbath, S., Fedo, C.M., Whitehouse, M.J., 2004. Characterization of Early Archean chemical sediments by trace element signatures. Earth Planet. Sci. Lett. 222, 43–60.
Byrne, R., Sholkovitz, E., 1996. Marine chemistry and geochemistry of the lanthanides. In: Gschneider Jr.K.A., Eyring, L. (Eds.), Handbook on the Physics and Chemistry of the Rare Earths. vol. 23. Elsevier, pp. 497–593.
Chen, Y.Z., Sang, B.L., Shao, G.Q., 1988. Geochemical characteristics of the late Archean iron-bearing series in the Huoqiu group of western Anhui province. Geochimica 4, 336–342 (in Chinese with English abstract).
Clayton, R.N., Mayeda, T.K., 1963. The use of bromine pentafluoride in the extraction of oxygen from oxides and silicates for isotopic analysis. Geochim. Cosmochim. Acta 27, 43–45.
Danielson, A., Moller, P., Dulski, P., 1992. The europium anomalies in banded iron formations and the thermal history of the oceanic crust. Chem. Geol. 97, 89–100.
Douville, E., Bienvenu, P., Charlou, J.L., Donval, J.P., Fouquet, Y., Appriou, P., Gamo, T., 1999. Yttrium and rare earth elements in fluids from various deep-sea hydrothermal systems. Geochim. Cosmochim. Acta 63, 627–643.
Ewers, W.E., Morris, R.C., 1981. Studies on the Dales Gorge member of Brockman iron formation. Econ. Geol. 76, 1929–1953.
Farquhar, J., Bao, H.M., Thiemens, M., 2000. Atmospheric influence of Earth's earliest sulfur cycle. Science 289, 756–758.
Farquhar, J., Cliff, J., Zerkle, A.L., Kamyshny, A., Poulton, S.W., Claire, M., Adams, D., Harms, B., 2013. Pathways for Neoarchean pyrite formation constrained by mass-independent sulfur isotopes. Proc. Natl. Acad. Sci. U. S. A. 110, 17638–17643.
Farquhar, J., Savarino, J., Airieau, S., Thiemens, M.H., 2001. Observation ofwavelength sensitive mass-dependent sulfur isotopes effects during SO2 photolysis: implication for the early Earth atmosphere. J. Geophys. Res. 106 (3), 2829–32839.
Fralick, P., Riding, R., 2015. Steep Rock Lake: sedimentology and geochemistry of an Archean carbonate platform. Earth-Sci. Rev. 151, 132–175.
Freslon, N., Bayon, G., Birota, D., Bollinger, C., Barrat, J.A., 2011. Determination of rare earth elements and other trace elements (Y, Mn, Co, Cr) in seawater using Tm addition and $Mg(OH)_2$ co-precipitation. Talanta 85, 582–587.
Geng, Y.S., Du, L.L., Ren, L.D., 2012. Growth and reworking of the early Precambrian continental crust in the North China Craton: constraints from zircon Hf isotopes. Gondwana Res. 21, 517–529.
German, C.R., Klinkhammer, G.P., Edmond, J.M., Mura, A., Elderfield, H., 1990. Hydrothermal scavenging of rare-earth elements in the ocean. Nature 345, 516–518.
German, C.R., Holliday, B.P., Elderfield, H., 1991. Redox cycling of rare earth elements in the suboxic zone of the Black Sea. Geochim. Cosmochim. Acta 55, 3553–3558.
Gnaneshwar Rao, T.G., Naqvi, S.M., 1995. Geochemistry, depositional environment and tectonic setting of the BIF's of the Late Archaean Chitradurga Schist Belt, India. Chem. Geol. 121, 217–243.
González, P.D., Sato, A.M., Llambías, E.J., Petronilho, L.A., 2009. Petrology and geochemistry of the banded iron formation in the Eastern Sierras Pampeanas of San Luis (Argentina): implications for the evolution of the Nogolí Metamorphic Complex. J. S. Am. Earth Sci. 28, 89–112.
Hoefs, J., 2009. Stable Isotope Geochemistry, sixth ed. Springer-Verlag, Berlin Heidelberg, pp. 285.
Hou, K.J., Li, Y.H., Zou, T.R., 2007. Laser ablation-MC-ICP-MS technique for Hf isotope microanalysis of zircon and its geological applications. Acta Petrol. Sin. 23 (10), 2595–2604 (in Chinese with English abstract).
Hou, K., Li, Y., Gao, J., Liu, F., Qin, Y., 2014. Geochemistry and Si-O-Fe isotope constraints on the origin of banded iron formations of the Yuanjiacun Formation, Lvliang Group, Shanxi, China. Ore Geol. Rev. 57, 288–298.
Huston, D.L., Logan, G.A., 2004. Barite, BIFs and bugs: evidence for the evolution of the Earth's early hydrosphere. Earth Planet. Sci. Lett. 220, 41–55.
Jahn, B.M., Zhang, Z.Q., 1984. Late Archean granulite gneisses from eastern Hebei Province, China: rare earth geochemistry and tectonic implications. Contrib. Mineral. Petrol. 85, 224–243.
James, H.L., 1954. Sedimentary facies of iron-formation. Econ. Geol. 49, 235–293.
Jiang, N., Guo, J.H., Zhai, M.G., Zhang, S.Q., 2010. Similar to 2.7 Ga crust growth in the North China craton. Precambrian Res. 179, 37–49.
Kato, Y., Kawakami, T., Kano, T., Kunugiza, K., Swamy, N.S., 1996. Rare-earth element geochemistry of banded iron formations and associated amphibolite from the Sargur belts, south India. J. SE Asian Earth Sci. 14, 161–164.
Kaufman, A.J., Johnston, D.T., Farquhar, J., Masterson, A.L., Lyons, T.W., Bates, S., Anbar, A.D., Arnold, G.L., Garvin, J., Buick, R., 2007. Late Archean biospheric oxygenation and atmospheric evolution. Science 317, 1900–1903.
Klein, C., 2005. Some Precambrian banded iron-formations (BIFs) from around the world: their age, geologic setting, mineralogy, metamorphism, geochemistry, and origins. Am. Mineral. 90, 1473–1499.
Klinkhammer, G.P., Elderfield, H., Edmond, J.M., Mitra, A., 1994. Geochemical implications of rare earth element patterns in hydrothermal fluids from mid-ocean ridges. Geochim. Cosmochim. Acta 58, 5105–5113.
Knauth, L.P., 2005. Temperature and salinity history of the Precambrian ocean: implications for the course of microbial evolution. Palaeogeogr. Palaeoclimatol. Palaeoecol. 219, 53–69.
Knauth, L.P., Lowe, D.R., 2003. High Archean climatic temperature inferred from oxygen isotope geochemistry of cherts in the 3.5 Ga Swaziland Supergroup, South Africa. Geol. Soc. Am. Bull. 115, 566–580.
Kröner, A., Cui, W.Y., Wang, W.Y., Wang, C.Q., Nemchin, A., 1998. Single zircon ages from high-grade rocks of the Jianping Complex, Liaoning Province, NE China. J. Asian Earth Sci. 16, 519–532.
Lalonde, S.V., Konhauser, K.O., 2015. Benthic perspective on Earth's oldest evidence for oxygenic photosynthesis. Proc. Natl. Acad. Sci. 112, 995–1000.
Lan, T.G., Fan, H.R., Santosh, M., Hu, F.F., Yang, K.F., Liu, Y., 2014. U-Pb zircon

chronology, geochemistry and isotopes of the Changyi banded iron formation in the eastern Shandong Province: constraints on BIF genesis and implications for Paleoproterozoic tectonic evolution of the North China Craton. Ore Geol. Rev. 56, 472–486.
Li, Y.H., Jiang, S., 1995. Silicon and oxygen isotope evidence for exhalative genesis of the Devonian Pb-Zn deposits in Feng-Tai region, Qinling Mountains, China. Chin. Sci. Bull. 40, 87–88.
Li, Y.H., Hou, K.J., Wan, D.F., 2010. Formation mechanism of Precambrian banded iron formation and atmosphere and ocean during early stage of the Earth. Acta Geol. Sin. 84, 1359–1373 (in Chinese with English abstract).
Li, Y.H., Hou, K.J., Wan, D.F., Zhang, Z.J., Yue, G.L., 2014. Precambrian banded iron formations in the North China Craton: silicon and oxygen isotopes and genetic implications. Ore Geol. Rev. 57, 299–307.
Liu, L., Yang, X.Y., 2015. Temporal, environmental and tectonic significance of the Huoqiu BIF, southeastern North China Craton: geochemical and geochronological constraints. Precambrian Res. 261, 217–233.
Liu, L., Yang, X., Santosh, M., Aulbach, S., 2015. Neoarchean to Paleoproterozoic continental growth in the southeastern margin of the North China Craton: Geochemical, zircon U-Pb and Hf isotope evidence from the Huoqiu complex. Gondwana Res. 28, 1002–1018.
Liu, L., Yang, X., Santosh, M., Zhao, G., Aulbach, S., 2016. U-Pb age and Hf isotopes of detrital zircons from the Southeastern North China Craton: Meso- to Neoarchean episodic crustal growth in a shifting tectonic regime. Gondwana Res. 35, 1–14.
Ludwig, K.R., 2003. User' s manual for Isoplot 3.0: a geochronological toolkit for Microsoft Excel. In: Berkeley Geochronology Center. Special Publication, vol. 4. pp. 1–71.
Ma, X.D., Fan, H.R., Santosh, M., Guo, J.H., 2014. Chronology and geochemistry of Neoarchean BIF-type iron deposits in the Yinshan Block, North China Craton: implications for oceanic ridge subduction. Ore Geol. Rev. 63, 405–417.
No.313 Geol. Team, 1991. A report of the regional 1:50000 geological survey in Huoqiu iron ore field. In: Anhui Bureau of Geology and Mineral Resources (in Chinese).
No.337, Geol. Team, 1986. A report of 1:50000 geological survey of the Sanhejian-Yunheji, Qiaogou-Gaotangji and Jiangji-Liuji Regions. In: Anhui Bureau of Geology and Mineral Resources (in Chinese).
Nozaki, Y., Zhang, J., Amakawa, H., 1997. The fractionation between Y and Ho in the marine environment. Earth Planet. Sci. Lett. 148, 329–340.
Nutman, A.P., Wan, Y.S., Du, L.L., Friend, C.R.L., Dong, C.Y., Xie, H.Q., Wang, W., Sun, H.Y., Liu, D.Y., 2011. Multistage late Neoarchaean crustal evolution of the North China Craton, eastern Hebei. Precambrian Res. 189, 43–65.
Olson, S.L., Kump, L.R., Kasting, J.F., 2013. Quantifying the areal extent and dissolved oxygen concentrations of Archean oxygen oases. Chem. Geol. 362, 35–43.
Ono, S., Eigenbrode, J.L., Pavlov, A.A., Kharecha, P., Rumble, D., Kasting, J.F., Freeman, K.H., 2003. Newinsights into Archean sulfur cycle from mass-independent sulfur isotope records from the Hamersley Basin, Australia. Earth Planet. Sci. Lett. 213, 15–30.
Ono, S., Kaufman, A.J., Farquhar, J., Sumner, D.Y., Beukes, N.J., 2009. Lithofacies control on multiple-sulfur isotope records and Neoarchean sulfur cycles. Precambrian Res. 169, 58–67.
Pavlov, A.A., Kasting, J.F., 2002. Mass-independent fractionation of sulfur isotopes in Archean sediments: strong evidence for an anoxic Archean atmosphere. Astrobiology 2 (1), 27–41.
Pecoits, E., Gingras, M.K., Barley, M.E., Kappler, A., Posth, N.R., Konhauser, K.O., 2009. Petrography and geochemistry of the Dales Gorge banded iron formation: paragenetic sequence, source and implications for palaeo-ocean chemistry. Precambrian Res. 172, 163–187.
Planavsky, N.J., Asael, D., Hofmann, A., Reinhard, C.T., Lalonde, S.V., Knudsen, A., Wang, X., Ossa Ossa, F., Pecoits, E., Smith, A.J.B., Beukes, N., Bekker, A., Johnson, T.M., Konhauser, K.O., Lyons, T.W., Rouxel, O.J., 2014. Evidence for oxygenic photosynthesis half a billion years before the Great Oxidation Event. Nat. Geosci. 7, 283–286.
Qi, R.Z., 1987. A discussion on the genesis of BIF of the Precambrian Huoqiu Group. Bull. Nanjing Inst. Geol. Miner. Resour. 8 (1), 1–20 (in Chinese with English abstract).
Qi, R.Z., Yao, G.Y., 1982. The metamorphism of Huoqiu Group. Bull. Nanjing Inst. Geol. Miner. Resour. 3 (3), 30–46 (in Chinese with English abstract).
Qiu, Y.Z., Yang, G.Y., 1982. The metamorphism of the Huoqiu Group. Bull. Nanjing Inst. Geol. Miner. Resour. 3 (3), 30–46 (in Chinese with English abstract).
Reinhard, C.T., Planavsky, N.J., Gill, B.C., Ozaki, K., Robbins, L.J., Lyons, T.W., Fischer, W.W., Wang, C.J., Cole, D.B., Konhauser, K.O., 2017. Evolution of the global phosphorus cycle. Nature 541, 386–389.
Riding, R., Fralick, P., Liang, L., 2014. Identification of an Archean marine oxygen oasis. Precambrian Res. 251, 232–237.
Robert, F., Chaussidon, M., 2006. A palaeotemperature curve for the Precambrian oceans based on silicon isotopes in cherts. Nature 443, 969–972.
Robinson, B.W., Kusakabe, M., 1975. Quantitative preparation of sulfur dioxide, for sulfur-34/sulfur-32 analyses, from sulfides by combustion with cuprous oxide. Anal. Chem. 47 (7), 1179–1181.
Shen, B., Zhai, A., Yang, C., Cao, X., 2005. Temporal-spatial distribution and evolutional characters of Precambrian iron deposits in China. Geol. Surv. Res. 28, 196–206 (in Chinese with English abstract).
Shen, B., Zhai, A., Chen, W., 2006. The Precambrian Mineralization of China. Geological Publishing House, Beijing, pp. 1–362.
Sholkovitz, E.R., Landing, W.M., Lewis, B.L., 1994. Ocean particle chemistry: the fractionation of rare earth elements between suspended particles and seawater. Geochim. Cosmochim. Acta 58, 1567–1579.
Slack, J.F., Grenne, T., Bekker, A., Rouxel, O.J., Lindberg, P.A., 2007. Suboxic deep seawater in the late Paleoproterozoic: evidence from hematitic chert and iron formation related to seafloor-hydrothermal sulfide deposits, central Arizona, USA. Earth Planet. Sci. Lett. 255, 243–256.
Sunder Raju, P.V., 2009. Petrography and geochemical behaviour of trace element, REE and precious metal signatures of sulphidic banded iron formations from the Chikkasiddavanahalli area, Chitradurga schist belt, India. J. Asian Earth Sci. 34, 663–673.
Thiemens, M.H., 1999. Mass-independent isotope effects in planetary atmospheres and the early solar system. Science 283, 341–345.
Trendall, A.F., 2002. The significance of iron formations (IF) in the Precambrian stratigraphic record. In: Altermann, W., Corcoran, P.L. (Eds.), Precambrian Sedimentary Environments: A Modern Approach to Ancient Depositional Systems. Special Publication of the International Association of Sedimentologists, vol. 33. pp. 33–66.
Wan, Y.S., Dong, C.Y., Wang, W., Xie, H.Q., Liu, D.Y., 2010. Archean basement and a Paleoproterozoic collision orogen in the Huoqiu Area at the Southeastern margin of North China Craton: evidence from sensitive high resolution ion micro-probe U-Pb zircon geochronology. Acta Geol. Sin. 84, 91–104 (English Edition).
Wan, Y.S., Dong, C.Y., Liu, D.Y., Kröner, A., Yang, C.H., Wang, W., Du, L.L., Xie, H.Q., Ma, M.Z., 2012. Zircon ages and geochemistry of late Neoarchean syenogranites in the North China Craton: a review. Precambrian Res. 222–223, 265–289.
Wang, W., Liu, S.W., Wilde, S.A., Li, Q.G., Zhang, J., Xiang, B., Yang, P.T., Guo, R.R., 2012. Petrogenesis and geochronology of Precambrian granitoid gneisses in Western Liaoning Province: constraints on Neoarchean to early Paleoproterozoic crustal evolution of the North China Craton. Precambrian Res. 222–223, 290–311.
Wang, C.L., Zhang, L.C., Lan, C.Y., Dai, Y.P., 2014. Petrology and geochemistry of the Wangjiazhuang banded iron formation and associated supracrustal rocks from the Wutai greenstone belt in the North China Craton: implications for their origin and tectonic setting. Precambrian Res. 255, 603–626.
Wonder, J., Spry, P., Windom, K., 1988. Geochemistry and origin of manganese-rich rocks related to iron-formation and sulfide deposits, western Georgia. Econ. Geol. 83, 1070–1081.
Wu, F.Y., Zhao, G.C., Wilde, S.A., 2005. Nd isotopic constraints on crustal formation in the North China Craton. J. Asian Earth Sci. 24, 523–545.
Wu, M.L., Zhao, G.C., Sun, M., Yin, C.Q., Li, S.Z., Tam, P.Y., 2012. Petrology and P-T path of the Yishui mafic granulites: implications for tectonothermal evolution of the Western Shandong Complex in the Eastern Block of the North China Craton. Precambrian Res. 222–223, 312–324.
Yang, X.Y., Liu, L., Lee, I., Wang, B., Du, Z., Wang, Q., Wang, Y., Sun, W., 2014. A review on the Huoqiu banded iron formation (BIF), southeast margin of the North China Craton: genesis of iron deposits and implications for exploration. Ore Geol. Rev. 63, 418–443.
Ying, J.L., Wang, Y.D., Zhao, F.Y., Lin, X.L., Sang, B.L., Xin, F.M., Chen, Y.Z., 1984. The geochronology study on Precambrian metamorphic rock from West Anhui. Geochimica 2, 145–152 (in Chinese).
Zhai, M.G., Santosh, M., 2011. The early Precambrian odyssey of the North China Craton. A synoptic overview. Gondwana Res. 20, 6–25.
Zhai, M.G., Santosh, M., 2013. Metallogeny of the North China Craton: link with secular changes in the evolving Earth. Gondwana Res. 24, 275–297.
Zhang, J., Nozaki, Y., 1996. Rare earth elements and yttrium in seawater: ICP-MS determinations in the East Caroline, Coral Sea, and South Fiji basins of the western South Pacific Ocean. Geochim. Cosmochim. Acta 60, 4631–4644.
Zhao, G.C., Zhai, M.G., 2013. Lithotectonic elements of Precambrian basement in the North China Craton: review and tectonic implications. Gondwana Res. 23, 1207–1240.
Zhao, G.C., Wilde, S.A., Cawood, P.A., Lu, L.Z., 1998. Thermal evolution of the Archaean basement rocks from the eastern part of the North China Craton and its bearing on tectonic setting. Int. Geol. Rev. 40, 706–721.
Zhao, G.C., Sun, M., Wilde, S.A., Li, S.Z., 2005. Late Archean to Paleoproterozoic evolution of the North China Craton: key issues revisited. Precambrian Res. 136, 177–202.
Zhao, G.C., Cawood, P.A., Wilde, S.A., Sun, M., Zhang, J., He, Y.H., Yin, C.Q., 2012. Amalgamation of the North China Craton: key issues and discussion. Precambrian Res. 222–223, 55–76.